ATLAS NOTE

ATLAS-CONF-2011-128

August 18, 2011

Particle Identification Performance of the ATLAS Transition Radiation Tracker

The ATLAS Collaboration

Abstract

The Transition Radiation Tracker (TRT) is the outermost charged particle tracking device of the ATLAS Inner Detector. In addition to its tracking capabilities, the TRT provides discrimination between electrons and pions over the energy range between 1 and 200 GeV by utilizing transition radiation. The electron identification is further improved using the measurement of the signal length that is sensitive to ionization loss. The same information can be used to search for highly ionizing new particles. In this note, we present the particle identification performance of the TRT detector during the first year of collision data-taking at $\sqrt{s}$ = 7 TeV.

1 Introduction

The ATLAS Inner Detector (ID) is composed of three detector sub-systems: the silicon-based Pixel and SemiConductor Tracker (SCT) detectors, and the gaseous drift tube Transition Radiation Tracker (TRT) [1]. The TRT is the outermost of the three sub-systems. It exploits a novel and unique design which combines continuous tracking capability with particle identification based on transition radiation. The latter functionality provides substantial discriminating power between electrons and pions over the energy range between 1 and 200 GeV and is a crucial component of the "tight" electron selection criteria in ATLAS [2]. The purpose of this note is to provide a detailed evaluation of the particle identification (PID) performance of the TRT observed in 7 TeV proton-proton collision data collected with the ATLAS detector at the Large Hadron Collider (LHC) in 2010.

Transition radiation (TR) is emitted when a highly relativistic charged particle with a Lorentz factor $\gamma \gtrsim 10^3$ traverses boundaries between materials of different dielectric constants. The active region of the TRT detector contains almost 300,000 straw drift tubes of 4 mm diameter. The space between the straws is filled with radiator material. The TR photons (soft X-rays) emitted in the radiator are absorbed in the gas inside the straw tubes, which serve as detecting elements both for tracking and for particle identification.

The TR-based electron-pion separation can be further enhanced at momenta $p \lesssim 10$ GeV through measurements of the time-over-threshold (ToT) of the straw signals, which vary as a function of energy deposition ($\mathrm{d}E/\mathrm{d}x$) in the straws. To achieve the best electron-pion separation, TR and $\mathrm{d}E/\mathrm{d}x$-based measurements are combined in a single likelihood function for a particle type. ToT measurements can also be used to to identify highly ionizing particles such as protons at low momenta, or hypothetical exotic objects such as highly ionizing stable massive particles [3].

This note is organized as follows. Section 2 summarizes the relevant details of the TRT detector. The data samples, electron, and pion reconstruction are explained in Section 3. Measurements of the TR and its application to the electron identification are presented in Section 4. This section also explains how the optimal hardware threshold settings were determined. Applications of the $\mathrm{d}E/\mathrm{d}x$ measurement are presented in Section 5. The particle identification performance using the combination of both TR and the $\mathrm{d}E/\mathrm{d}x$ measurement is shown in Section 6.

2 Transition Radiation Tracker

The TRT is a straw tracker composed of 298,304 carbon-fibre reinforced Kapton® straws, arranged in a barrel and two symmetrical end-cap configurations [4]. The barrel section covers $560 < R < 1080$ mm and $|z| < 720$ mm and has the straws aligned parallel to the direction of the beam axis [5].[1] The two end-cap sections cover $827 < |z| < 2744$ mm and $617 < R < 1106$ mm and have the straws arranged in wheels. The end-cap straws are aligned perpendicular to the beam axis, pointing outwards in the radial direction [6]. The TRT extends up to pseudo-rapidity $|\eta| = 2$. The average number of TRT hits on a track is about 34, except in the transition region between barrel and end-caps and at $|\eta| > 1.7$ where it is reduced to approximately 25. For a radiator material, polypropylene fibres are used in the barrel and polypropylene foils in the end-caps. The straws are filled with a gas mixture of 70% Xe, 27% CO_2 and 3% O_2. Xenon is used for its high efficiency to absorb TR photons of typical energy $6 - 15$ keV. The

[1] ATLAS uses a right-handed coordinate system with its origin at the nominal interaction point (IP) in the centre of the detector and the z-axis coinciding with the axis of the beam pipe. The x-axis points from the IP to the centre of the LHC ring, and the y-axis points upward. Cylindrical coordinates (R, ϕ) are used in the transverse plane, ϕ being the azimuthal angle around the beam pipe and R the distance from the beam pipe in the radial direction. The track pseudo-rapidity is defined as $\eta = -\ln(\theta/2)$, where the polar angle θ is the angle between the track direction and the z axis.

combined probability for production, absorption and detection of a TR photon is about 20% per hit for an electron above TR threshold.

The TRT operates as a drift chamber: when a charged particle traverses the straw, it ionizes the gas, creating about 5-6 primary ionization clusters per mm of path length. The straw wall is held at a potential of -1530 V with respect to a 31 μm diameter gold-plated tungsten wire at the center that is referenced to ground. The electrons drift towards the wire and cascade in the strong electric field very close to the wire, thus producing a detectable signal. The signal on each wire is amplified, shaped and discriminated against two adjustable thresholds, a low threshold (LT) at about 300 eV and a high threshold (HT) at about $6-7$ keV [7]. The two thresholds are needed in order to measure the tracking information as well as to identify a large energy deposit due to the absorption of a TR photon. For any triggered event, the TRT reads out data over three bunch crossing periods, 3×25 ns. The measured drift times span a range of about 50 ns. The information about whether the low threshold is exceeded or not is measured separately in time intervals of 3.12 ns length so that each crossing period is divided into eight time bins. The first low threshold $0 \rightarrow 1$ transition marks the leading edge (LE) of the signal (hit), and the leading edge time t_{LE} is defined as the centre of the first bin set to "1". Similarly, the last $1 \rightarrow 0$ transition is called the trailing edge (TE) of the hit. The information about whether the HT is exceeded or not is recorded at a coarser granularity, every 25 ns. A hit is said to be a HT hit if any of the three HT bits is high.

The leading (trailing) edge time depends on the time when the closest (furthest) electron cluster arrives at the wire at the center of the straw. The leading edge time is thus directly related to the track-to-wire distance r_{track} [8]. If the furthest electrons were always produced at the straw wall and drifted for the full straw radius of 2 mm, t_{TE} time would be independent of r_{track}. This, however, is not the case, due to the finite interaction length (and thus the limited number of primary ionization clusters) and signal shaping effects. A particle that deposits more ionization inside the straw will on average have a higher signal, exceed the threshold sooner, have signal above threshold for longer, and hence also earlier LE, later TE and longer ToT. This correlation can be used to obtain a ToT-based $\mathrm{d}E/\mathrm{d}x$ estimate.

3 Data samples and track reconstruction

Data from proton-proton collisions at the LHC at $\sqrt{s} = 7$ TeV recorded by the ATLAS detector in 2010 were used for the studies reported in this note. The detector response for electrons was studied with samples of reconstructed photon conversions and Z boson decays. Different triggers and data sets were used to reconstruct the electron candidates from the two sources. The detector response to pions was studied using the same data set as for photon conversions.

The results observed in data were compared to Monte Carlo (MC) simulations [9]. The detector response to electrons from photon conversions and pions in data were compared to Pythia non-diffractive minimum bias MC simulation. The electrons from Z boson decays were compared to Pythia $Z \rightarrow ee$ MC simulation.

The ATLAS detector simulation primarily uses the `GEANT4` framework [10]. For the TRT, however, the default simulation of a charged particle passing through the very thin gas layers was shown to be inaccurate. Customized standalone packages called the Transition Radiation model and Photon Absorption and Ionization model (PAI) are used instead for the creation of transition radiation and to simulate the energy loss of charged particles due to ionization, respectively.

The data-taking periods and trigger requirements are summarized in more detail in Section 3.1 below. Sections 3.2 through 3.4 explain the reconstruction of electrons from photon conversions, electrons from Z boson decays, and pions, in that order. The purity of these samples is discussed in Section 3.5.

3.1 Data periods and trigger requirements

A minimum bias trigger was used to record the data set used for the reconstruction of photon conversions and pion candidates. During the initial low-luminosity running period from April 15 to June 5, 2010, the events were collected in the minimum bias trigger stream at a rate that was typically between 40 Hz and 200 Hz, providing a high statistics sample of electrons from photon conversions. This data set corresponds to an integrated luminosity of approximately $\int \mathcal{L}\,dt = 9\,\text{nb}^{-1}$.

Data recorded during June 24, 2010 - October 29, 2010, corresponding to an integrated luminosity of $\int \mathcal{L}\,dt = 35\,\text{pb}^{-1}$, was used to reconstruct electron candidates from Z boson decays. Events were required to be triggered by an electron trigger that has close to 100% efficiency for electrons from Z boson decays selected in this analysis.

The LHC bunch spacing during both running periods was 150 ns or greater. Pile-up from multiple interactions per bunch crossing was small. The average number of minimum bias interactions per beam crossing was less than 0.2 in the data set used for photon conversions, and about three in the data set used to reconstruct the sample of Z bosons.

Good data quality requirements were applied to all data as follows. The Inner Detector tracking system that is needed for accurate conversion finding was required to be fully functional. The calorimeter information used to identify Z boson decays to two electrons was required to be of high quality.

3.2 Electron candidates from photon conversions

Photon conversions to electron-positron pairs were used to reconstruct a pure sample of electrons. The photon conversion candidates [11] are required to have two tracks, each with a minimum of 20 TRT hits and four silicon (SCT and Pixel) hits. The vertex is required to be well reconstructed and to be at least 60 mm away from the primary vertex in the radial direction. To improve the sample purity, a tag and probe method is applied to the two tracks of the selected photon conversion candidates. The tag leg is required to have a ratio of the number of TRT high-threshold hits to total TRT hits of at least 0.12, which corresponds to at least three high-threshold hits on a track with the minimum total number of 20 TRT hits. For a conversion candidate passing these requirements, the probe leg is declared to be an electron candidate. The two tracks are treated independently; if both of the tracks pass the tag requirement, each is also used as a probe. Over 500,000 electron candidates satisfy these selection criteria, providing a high statistics sample of electron candidates at the early stages of collision data-taking. Figure 1 shows the momentum distribution of the electron candidates. The corresponding range of γ is about $10^3 - 10^4$.

3.3 Electron candidates from Z boson decays

A second sample of electron candidates is obtained from the reconstruction of $Z \to ee$ decays. Electrons from this sample have higher momenta, and can thus be used to probe the TR performance at higher values of γ. Electron candidates are required to pass the calorimeter based "medium" electron selection criteria [2], and to have an innermost Pixel layer (b-layer) hit when passing through an active part of the b-layer. Candidate events are required to have two such electrons, with a reconstructed di-lepton invariant mass in the range 75 – 105 GeV. Electrons from Z boson decays are treated in the same way as those from photon conversions. The tag leg is required to have a TRT high-threshold ratio greater than 0.12, and both the tag and the probe leg are required to have at least 20 TRT hits. The momentum distribution of electron candidates from Z boson decays is shown in Fig. 1. The corresponding values of the γ factor are around 10^5.

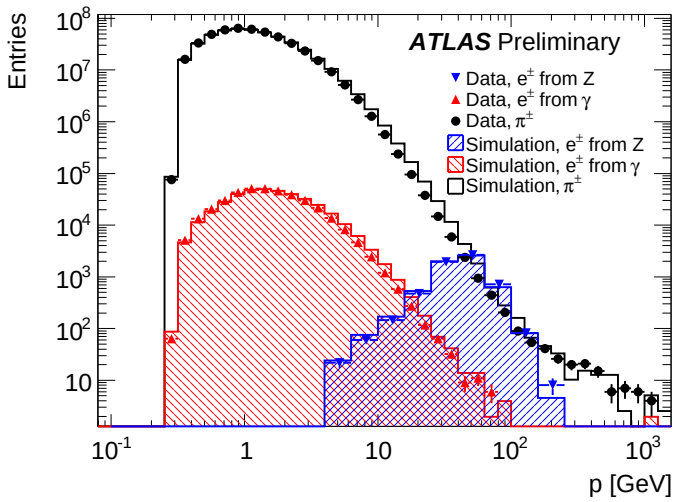

Figure 1: Momentum distribution for electron candidates from photon conversions, electrons from Z boson decays and pion candidates. The distribution for the MC simulation sample is rescaled to the number of entries observed in data.

3.4 Pion candidates

Pion candidates are selected from reconstructed particle tracks that have a minimum of 20 TRT and four silicon hits. Further selection criteria are applied to reject electrons, protons and kaons. Any track that does not have a hit in the innermost Pixel layer or that is reconstructed as a part of a photon conversion candidate is excluded. Photon conversion candidates include track pairs in which only one of the tracks has silicon hits as well as single-track conversion candidates. These two requirements reduce electron contamination from photon conversions, which is the dominant source of electrons in the minimum bias data. Additionally, any track with $\mathrm{d}E/\mathrm{d}x$ above 1.6 $\mathrm{MeVg^{-1}cm^2}$ in the Pixel detector is excluded in order to reduce the contamination from protons (and to a lesser extent kaons) at low momentum [12]. A track passing these requirements is declared to be a pion candidate. The momentum distribution of the pions is similar to that of the electron candidates from photon conversions shown in Fig. 1. The γ factors are however calculated assuming the pion mass, and are in the range from about 2 to 200 in the barrel, and 2 to 700 in the end-caps.

3.5 Purity of the reconstructed track samples

The purity of the electron candidates from conversions and pion candidates from generic tracks was studied with the simulated sample. The results as a function of γ are shown in Fig. 2. As in the rest of this note, the value of γ is calculated using the assumed mass of the candidate (electron or pion), which is systematically different from the true γ factor for misidentified candidates. For electron candidates in the TRT barrel region, the simulation estimates that the sample purity is higher than 99% for $\gamma < 10^4$. At higher values of γ, the contamination from pions increases to about 2%. In the end-cap region, the simulation estimates that the contamination from pions and other hadrons increases with increasing γ factor, from below 1% for $\gamma \lesssim 2 \cdot 10^4$ to around 5% at $\gamma \approx 4 \cdot 10^4$. For the electron candidates the effect of the contamination from pions (and more generally all hadrons) will result in a lower average HT fraction. The systematic negative bias is equal to the pion contamination, multiplied by the difference in HT fraction for electron and pion tracks. This bias is negligible, except at high values of γ in the end-cap,

where the average HT fraction for all electron candidates is 0.01 lower than for true electrons.

The purity of pion candidates is considerably lower. The overall composition of the pion sample, combining barrel and end-caps and summed over all momenta, is 84% pion, 10% kaon and 5% proton. The fraction of pions is above 90% for $\gamma < 5$. The contamination from electrons, which would emit transition radiation at the same momenta, is less than 0.5%. The contribution of charged kaons and protons becomes significant for γ factor above 5 and 10 respectively, as the Pixel $\mathrm{d}E/\mathrm{d}x$ measurement becomes less discriminating. For $\gamma > 20$, the sample composition is approximately constant at about 65% pions, 25% kaons, and 10% protons. However, this mixed sample still provides an accurate model of the high threshold response for pions since the response for kaons and protons is similar to pions in this range. The positive bias on the measured average HT fraction due to electron contamination is found to be negligible.

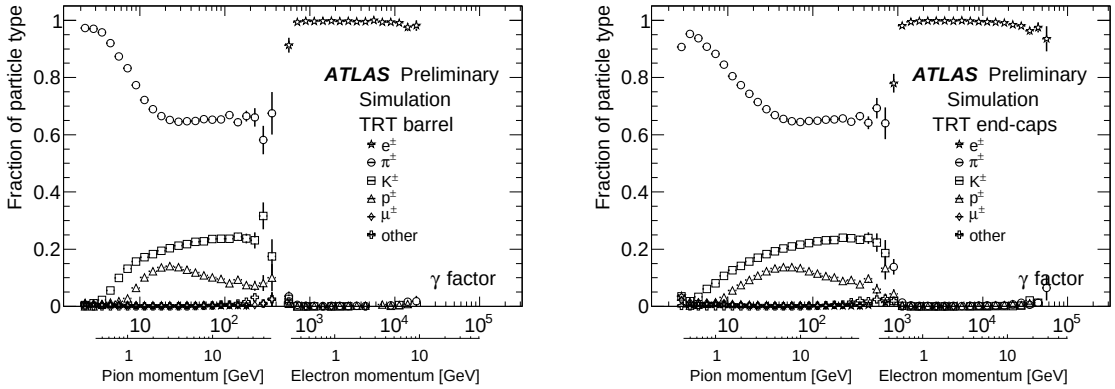

Figure 2: The reconstructed track sample composition for the barrel (left) and end-caps (right), as a function of the Lorentz γ factor. The value of γ is calculated using the assumed mass of the candidate (electron or pion). The composition is estimated from truth information in the MC simulation. The same track reconstruction and selection as in data is used.

4 Transition radiation and high threshold hits

This section presents the results of HT studies in electron and pion samples. Figure 3 shows the HT fraction distributions for electron and pion candidates. The HT fraction is defined as the fraction of hits on track that exceed the high threshold. The distribution for electrons shown in Fig. 3 is clearly shifted to higher values. The HT probability shown later in this section is defined as the average HT fraction.

Section 4.1 shows the HT probability dependence on the γ factor. Section 4.2 presents detailed studies of the variation of the HT probability within the detector. The differences between the data and simulated samples shown in Sections 4.1 and 4.2 are discussed at the end of those sections. Section 4.3 shows the performance of a requirement on the HT fraction, in terms of the electron efficiency and pion misidentification probability. Section 4.4 explains how the hardware HT setting was validated with 7 TeV collision data.

4.1 Transition Radiation onset

The first step towards establishing electron identification with the TRT is to observe the expected increase in the average number of HT hits with γ. The increase has been observed in 2004 test-beam data [13],

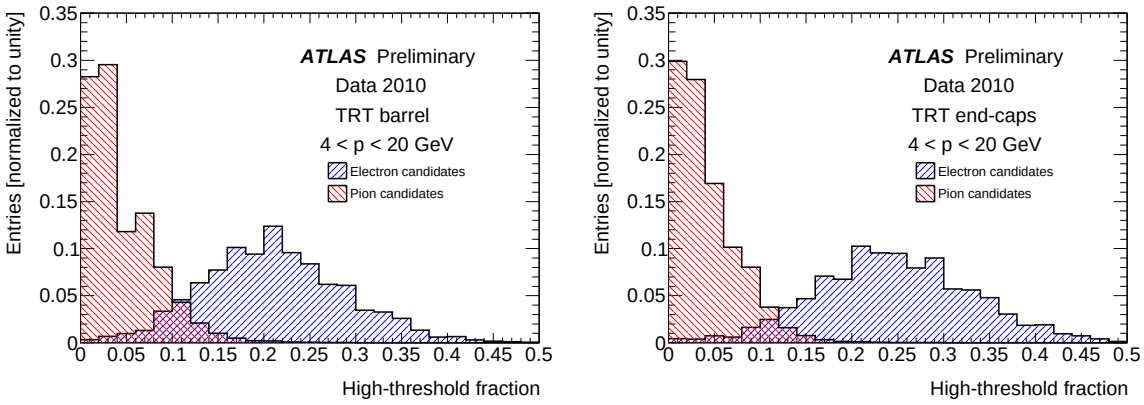

(a) tracks with at least 20 barrel hits

(b) tracks with at least 20 end-cap hits

Figure 3: The HT fraction for electrons from photon conversions and pion candidates in momentum range 4 GeV $< p <$ 20 GeV, in barrel (a) and end-cap (b) regions.

cosmic-ray data [14] and for collision data at $\sqrt{s} = 900$ GeV [15]. The HT probability observed in 7 TeV collision data is shown in Fig. 4 and agrees well with earlier measurements.

The results are shown separately for five intervals in pseudo-rapidity η reflecting different detector regions. The errors are statistical only. The average HT fraction was evaluated for tracks in bins of the Lorentz factor γ. The pions, electrons from photon conversions and electrons from Z boson decays cover different γ ranges. For the electron candidates, the sharp turn-on of the transition radiation can be seen, with the HT probability increasing rapidly from 0.05 to a plateau of $0.2 - 0.3$ as γ increases from 600 to 5000 and above. The HT plateau level in the end-cap region is higher than in the barrel. The HT response in different detector regions will be discussed in more detail in the next section. Electrons from the reconstructed Z decays allow studies of HT probability at $\gamma \approx 10^5$, which can not be accessed with electrons from photon conversions. Small differences in the HT probability for the electrons from conversions and $Z \to ee$ decays in the overlapping γ range can not be resolved at the current statistical uncertainty. The lower HT probability for the electrons from conversions at $|\eta| > 1.07$ could be due to the higher pion contamination in the end-cap region.

The pion candidates shown in Fig. 4 populate the region $\gamma < 10^3$. In this γ range, HT hits are caused by large ionization energy deposits due to Landau $\mathrm{d}E/\mathrm{d}x$ fluctuations. Such fluctuations exist also for electrons with $\gamma > 10^4$ and contribute there about 0.08 to the HT probability. The HT probability for pion candidates increases gradually from about 0.04 at $\gamma \approx 1$ to about 0.07 at $\gamma \approx 700$ ($p \approx 100$ GeV) due to the rise of $\langle \mathrm{d}E/\mathrm{d}x \rangle$ with increasing track momentum. This behavior was cross-checked with a sample of pion candidates from K^0_s decays that has higher pion purity, and the results were in good agreement.

Figure 4 includes also the result obtained for the simulated events, analyzed in the same way as the data sample. The agreement between data and MC simulation is best in the barrel region, where the simulation response was tuned based on the ATLAS combined test-beam data [13]. Only barrel modules were tested in the test beam. The HT probability for pions is overestimated by about 10% in MC samples. The HT probability due to TR for electrons in the end-caps is underestimated in simulation, by up to 20%. Both effects contribute to a better electron-pion separation in data, when compared to MC expectations. The MC simulation has since been tuned to better describe the data. The updated tuning will be used for the next production of simulated events, expected for autumn 2011.

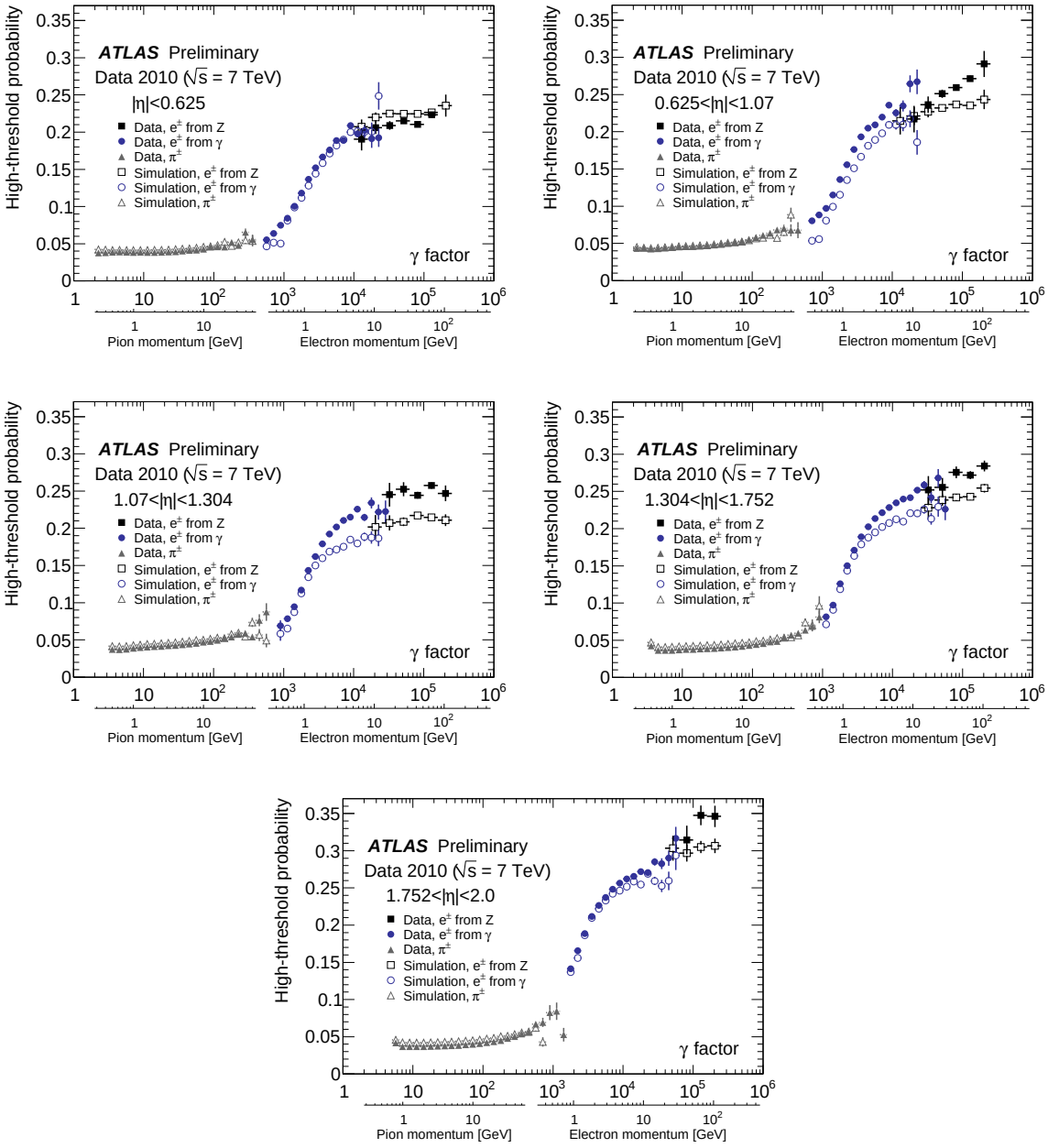

Figure 4: The high-threshold turn-on curve, separated into regions according to the reconstructed track η. The value of Lorentz γ factor is calculated using the assumed mass of the candidate (electron or pion).

4.2 Geometrical variation

This section reports results of studies of the HT probability on a finer detector granularity. The section starts with an explanation of the detector geometry that is important for the understanding of the results.

The straws are assembled in modules in the barrel, and wheels in the end-cap region. Within the modules (wheels), the straws are arranged in straw layers. In the barrel, where straws are parallel to the

beam axis (z direction), the same straw extends from $z = -720$ mm to $z = 720$ mm. Glass wire joints at $z = 0$ mechanically connect two electrically separated wires and each side is read out separately. Wires in the innermost nine out of 73 straw layers of the barrel are split into three parts, where the central section at $|z| < 400$ mm is not read out. These straws are referred to as "short" straws. The straw layer number increases with increasing distance from the beam pipe.

In the end-caps, there are two types of wheels that differ in the spacing between the straw planes and in the number of straws per wheel. Type A wheels at smaller $|z|$ have smaller spacing and twice the number of straw layers when compared to type B wheels. The straw layer number increases with increasing $|z|$. There are six A-wheels with 16 straw layers each, and eight B-wheels with eight straw layers each, giving 160 straw layers in total.

The HT probability as a function of the straw layer for electron and pion candidates, averaged over all hits on track in a given straw layer, is shown in Figure 5. All electron candidates from photon conversions with momenta above 2.5 GeV are used for this study. A tighter requirement on the momentum would result in a too small sample of electron candidates. Electrons in this momentum range are close to being on the HT plateau region. The related negative systematic bias on HT probability due to the variation in HT response with γ is about 1%. The systematic bias was estimated by comparing the HT probability to that obtained from the electrons in momentum range of 4 GeV $< p <$ 20 GeV.

The mechanical structure of the detector can be seen. The HT probability in the electron sample is the

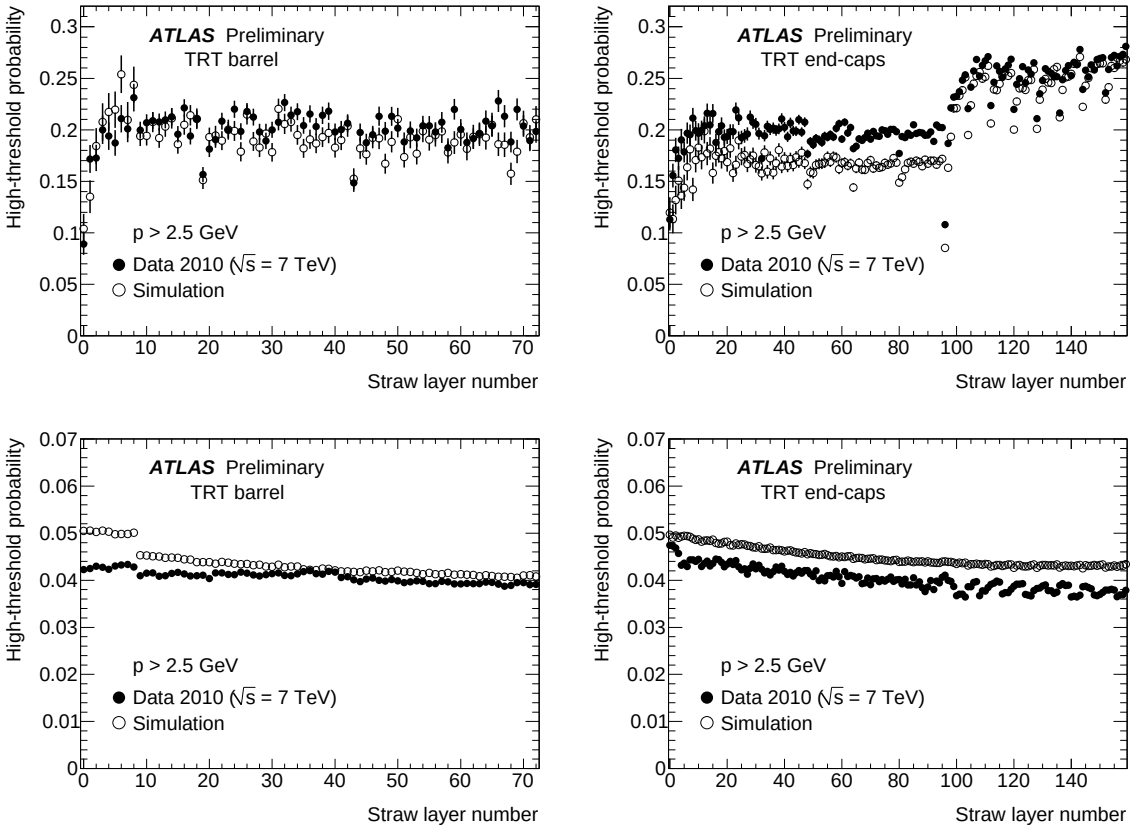

Figure 5: The HT probability for electron (top) and pion (bottom) candidates as a function of straw layer number in the TRT barrel and end-caps. Increasing straw layer corresponds to increasing the radial distance from the beam pipe in the barrel and increasing $|z|$ in the end-caps.

largest in the end-cap B-wheels, which have larger spacing when compared to the A-wheels, and hence more radiator material between straws. In each detector region, the HT probability increases to a plateau over the first few straw layers. The TR yield saturates after $2-3$ straw layers, as equilibrium is reached between generation and absorption of TR photons. In the barrel, a sharp decrease in the HT probability for electron candidates is observed in straw layers 0, 19 and 43, which correspond to the first straw layer of each barrel module. In the end-caps, the decrease is observed for the first straw layer of each wheel: every 16 straws in A-wheels, and every eight straws in B-wheels. The effect is more pronounced in the B-wheels, where there are only eight straw layers per wheel.

The HT probability for the pion candidates is observed to decrease as the straw layer number increases in both the barrel and the end-caps. The HT hits for pions that are below the TR threshold are caused by large ionization energy deposits ($\mathrm{d}E/\mathrm{d}x$). The main parameter that affects the ionization loss is the track length within the straw. When a track passes a straw at a larger angle, the track path length inside the straw is longer, charge deposition is larger, and the probability for the signal to exceed the high threshold increases. In the barrel region, the track η range decreases with increasing straw layer number (R). The track length within the straw as well as the HT probability therefore decrease as well, as observed in Fig. 5. In the end-caps, the track η range increases with increasing straw layer number. Due to different orientations of the straws, this again results in the decrease in HT probability as the straw layer number increases. The first nine straw layers in the barrel have systematically higher HT probability because they are active only for $|z| > 400\,\mathrm{mm}$, and therefore the average track η as well as the track length within the straw is larger.

Other effects that can impact the observed HT probability for pions are the momentum dependence from the relativistic increase in ionization loss at higher momenta, signal attenuation along the length of the straw, signal reflection from the end of the wire without electronics, and variations in electronic threshold. A small residual structure that is limited to groups of four consecutive straw layers in the end-caps can be minimized with fine hardware setting corrections.

In the azimuthal direction, the detector read-out is segmented in 32 ϕ sectors. A study of HT probability for different ϕ sectors confirmed there is no significant dependence, either for electrons or for the pion candidates.

The geometrical variation in HT probability observed in the data is reproduced by the simulation. For electrons, the HT probability is underestimated in simulation by about 20% in the end-cap A-wheels. For pions, the increase in HT probability in barrel short straws is overestimated in simulation. The simulation reproduces the decrease in HT probability in the first few straw layers of each module or wheel.

4.3 Electron efficiency and pion misidentification probability

The HT-based electron-pion separation demonstrated in Fig. 3 is utilized by a requirement of a minimum HT fraction for electron candidates. Figure 6 shows the fraction of electron and pion candidates that pass a HT fraction selection requirement, in bins of $|\eta|$. All electron candidates from photon conversions with momentum in range $4\,\mathrm{GeV} < p < 20\,\mathrm{GeV}$ are used for this study. The pion misidentification probability $p_{\pi\to e}$ is the probability for a pion to pass an electron HT fraction selection criteria. The pion rejection power is $1/p_{\pi\to e}$. A direct comparison of the electron efficiency and the pion misidentification probability from Fig. 6 is included in Fig. 7. The uncertainty on the pion misidentification probability shown in Fig. 7 (b) was estimated by varying the selection criteria such that the electron efficiency changed by $\pm 2\%$. The range of $\pm 2\%$ is sufficiently big to include the uncertainties due to hadron contamination in the electron sample of about 1%.

The minimum HT fraction that is required for an electron to pass the ATLAS "tight" electron selection requirement [2], the corresponding efficiency for electrons to pass this criterion as well as the pion misidentification probability are summarized in Table 1. The current HT fraction selection criterion was

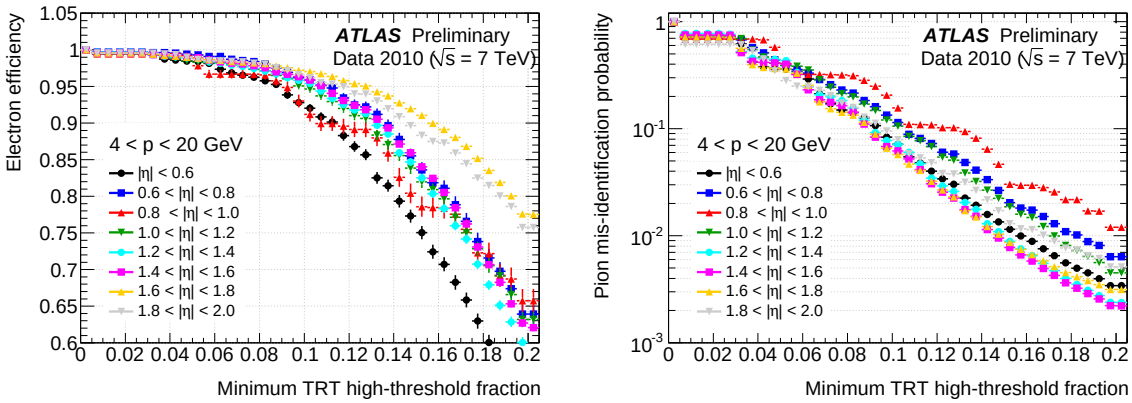

Figure 6: The fraction of electron (left) and pion (right) candidates that pass a given HT fraction selection, as a function of that criterion. The "steps" in the transition region at $0.8 < |\eta| < 1.0$ are due to the discrete distribution of the number of HT hits on track in the region where the spread in the number of all hits on tracks is small.

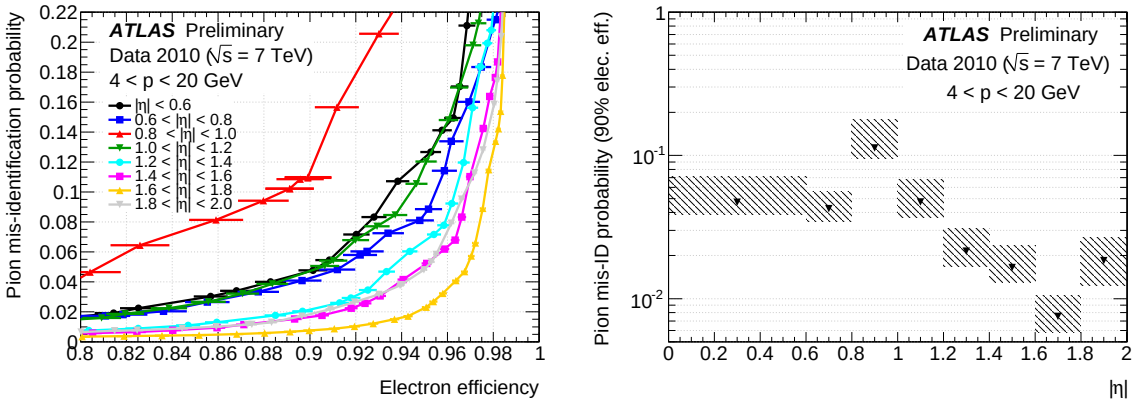

(a) (b)

Figure 7: Fraction of pion candidates versus fraction of electron candidates passing given HT fraction criteria (a); points along the lines represent different criteria. Pion misidentification probability for HT fraction criteria that give 90% electron efficiency (b), determined separately in different η bins.

determined based on MC studies prior to the start of collision data-taking, and was chosen such that a pion rejection factor of at least 10 would be achieved after applying the HT fraction electron selection criteria [1]. In the range $0.625 < |\eta| < 1.07$, only a factor of four was achieved due to fewer hits on track in the transition region and a relatively large HT hit probability for pions for geometric reasons. In the highest η bin, the pion rejection factor is almost 100.

4.4 Validation of hardware high threshold setting

In order to determine the optimal average high threshold setting, data corresponding to an integrated luminosity of $20\,\text{nb}^{-1}$ were taken with different HT settings in July 2010, and the results of the pion rejection study with different settings are reported in this section. An electron trigger that maximized the number of reconstructed photon conversion candidates was used to record these data.

$\|\eta\|$ range			Minimum HT fraction	Electron efficiency	Pion misidentification probability
0.0	→	0.625	0.085	0.953 ± 0.004	0.1268 ± 0.0003
0.625	→	1.07	0.085	0.961 ± 0.005	0.2420 ± 0.0004
1.07	→	1.304	0.115	0.921 ± 0.005	0.0473 ± 0.0001
1.304	→	1.752	0.13	0.919 ± 0.002	0.0174 ± 0.0001
1.752	→	2.0	0.155	0.882 ± 0.002	0.0109 ± 0.0001

Table 1: Minimum HT fraction selection criteria that are applied to "tight" electrons. The fraction of electron and pion candidates that pass this selection criteria are also shown. The quoted errors are statistical only.

The value of the high threshold can be varied by changing the Digital to Analogue Converter setting (DAC counts) on the Amplification, Shaping, Discrimination, and Base-Line Restoration (ASDBLR) chip [7], in steps of about 60 eV. Prior to the start of collision data-taking, the average HT was adjusted to the setting that gave the best performance at the test beam. Results from electronics noise scans were used to correct for the large variations in response due to variations in ground offsets. Corrections to these HT settings were considered on three different detector granularities:

- full detector to determine the optimal average HT setting;
- straw layer variations, to minimize the variation due to the variation with the track incidence angle and other small effects;
- equalization of HT settings on ASDBLR level, to avoid small-level granularity variations.

Only the validation of the average HT setting for the full detector is reported in this note. To validate the average HT setting, data were recorded with six different HT settings: nominal settings, ±15 DAC counts from nominal, ±25 DAC counts from nominal, and −8 DAC counts from nominal. The high-threshold settings were varied uniformly across the entire detector.

The HT probability as a function of the difference in HT settings is shown in Fig. 8 for electron and pion candidates with 4 GeV $< p <$ 20 GeV. As the threshold is decreased, the HT probability increases for both electron and pion candidates. The pion HT probability is similar for the barrel and end-cap A and B-type wheels. The electron HT probability is similar for barrel and end-cap A-type wheels, but 0.05 (20% relative) higher for end-cap B-type wheels, consistent with the results reported in Section 4.

The optimal average HT setting is determined based on the pion rejection power. The HT fraction selection criteria that gives 90% electron efficiency was determined for different values of high threshold settings and for different η bins. Figure 9 shows the efficiency for a pion candidate to pass the selection criteria as a function of the high threshold setting difference. The selection criteria at 90% electron efficiency was used as a reference for this study. As in Section 4.3, the uncertainties were estimated by varying the selection criteria such that the electron efficiency changed by ±2%. For all η regions, the pion misidentification probability $p_{\pi\to e}$ is independent of the HT setting in the range of -25 to nominal DAC count. For settings higher than nominal, $p_{\pi\to e}$ increases. Based on these results, the high-threshold was lowered by eight DAC counts across the detector for 2011 data-taking. The primary reason for lowering the thresholds was to operate at stable settings, where the performance does not vary much if the HT is slightly above or below the nominal.

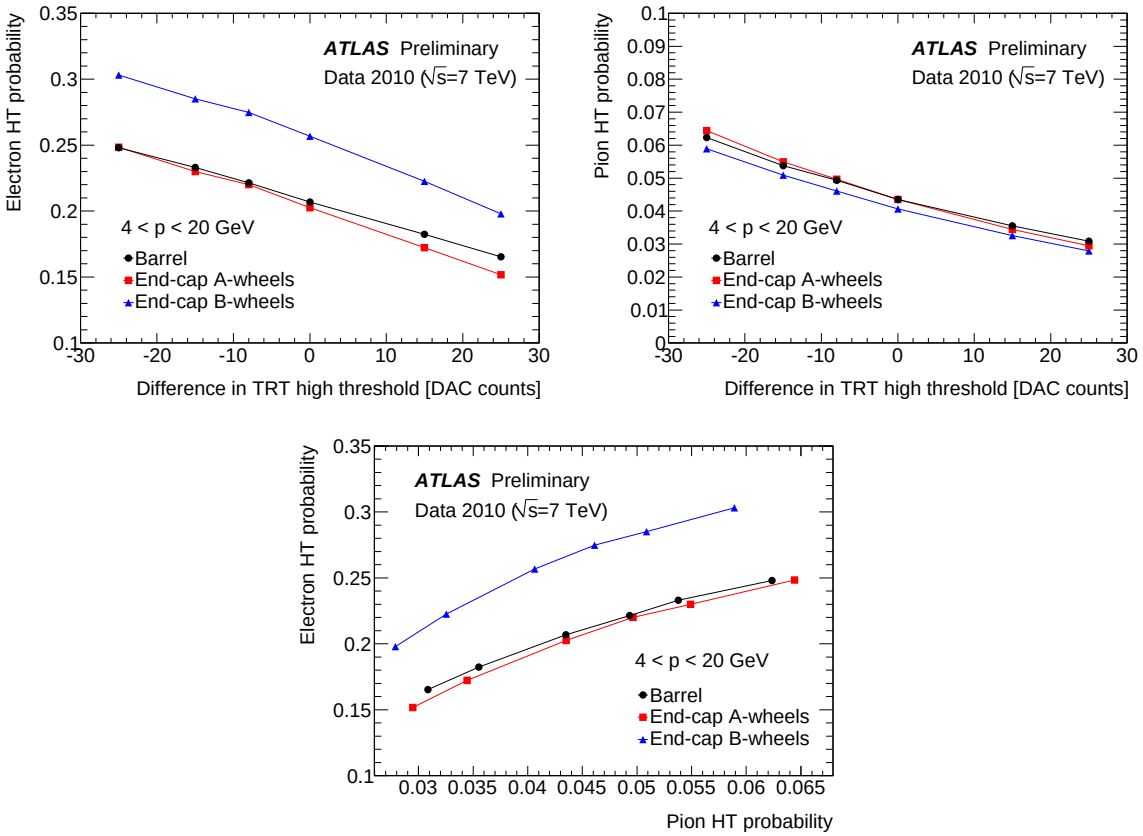

Figure 8: The electron and pion probability dependence on the change in HT setting (top left and right) and the HT probability for electrons vs. the HT probability for pions (bottom). The results for different regions of the detector are shown separately.

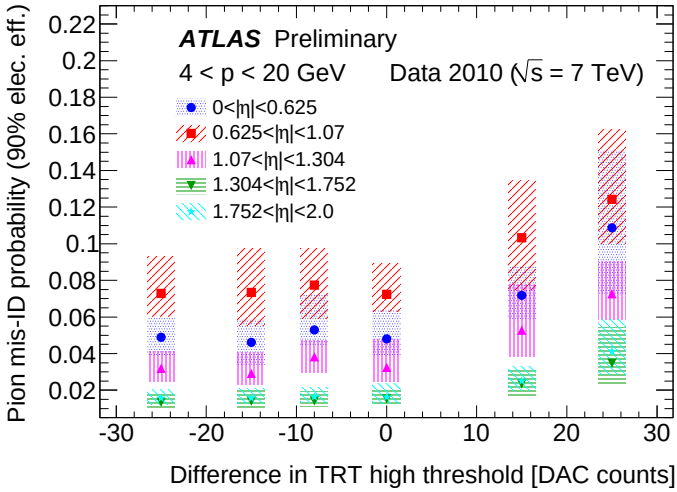

Figure 9: Pion misidentification probability at 90% electron efficiency as a function of a change in high threshold setting for different η ranges.

5 Time over threshold based particle identification

The measured time over threshold is correlated with the ionization deposit within the straw, and can thus be used to better distinguish between electrons and pions based on their expected $\mathrm{d}E/\mathrm{d}x$. Similar discriminators based on TRT timing information can be used to distinguish between other types of particles, such as protons, kaons and hypothetical highly ionizing exotic particles.

A ToT-based variable that is somewhat different from the full signal length of $t_{\mathrm{TE}} - t_{\mathrm{LE}}$ is used for the $\mathrm{d}E/\mathrm{d}x$ measurement. This variable takes into account the possibility for the signal from the deposited ionization to temporarily fall below threshold, breaking the full hit in two:

`00000011 11111101 1111000`.

This is less likely to happen when the ionization deposit is larger. For the purpose of the $\mathrm{d}E/\mathrm{d}x$ measurement, the ToT is defined as the number of bits above threshold in the largest single group of bits above threshold, multiplied by the bin width, $8 \times 3.12\,\mathrm{ns}$ for the example shown above. This method has a similar performance to a method that uses all bits above threshold, and a better performance than a method that uses $t_{\mathrm{TE}} - t_{\mathrm{LE}}$.

The ToT is subject to several systematic effects that are not related to $\mathrm{d}E/\mathrm{d}x$. The t_{LE} depends on the track-to-wire distance due to the drift time. Due to the limited number of primary ionization clusters, the t_{TE} also depends on the track-to-wire distance. The track-to-wire distance related variation in the measured ToT is about 10 ns. Other smaller effects that can cause variations of a few ns along the wire length are signal attenuation (attenuation length $\lambda = 4\,\mathrm{m}$ [4]), signal reflection from the end of the wire that is not read out, signal delay due to the propagation along the wire and signal shaping.

These effects are taken into account by corrections that vary with the track-to-wire distance and distance along the straw. The track-to-wire distance dependent corrections also take into account the dependence of the total energy deposit within the straw on the track length. For particles originating from the interaction point, the track incidence angle (or pseudo-rapidity η) is strongly correlated with its position along the wire. Therefore, η-dependent corrections can be used instead of the distance along the straw dependent corrections.

5.1 Electron identification

The ionization loss for electrons and pions differs the most for particles of low momentum, $p < 10$ GeV. This momentum range is where the ToT-based electron-pion separation contributes most to the overall electron identification performance. To achieve the best sensitivity, all systematic effects discussed in the first part of Section 5 need to be taken into account. Corrections are made for z dependence in the barrel and R dependence in the end-caps. To take into account the track-to-wire distance dependence, the average corrected ToT measurement is divided by the average track-to-wire distance. Future studies will use a more accurate hit-level correction that was developed after the start of collision data-taking. The track level ToT-based discriminator is obtained by averaging corrected ToT measurements for all hits on track that do not exceed the HT. The HT hits are not used in order to avoid the correlation between the ToT-based variable and the HT fraction. Figure 10 shows the corrected ToT distributions for the electron and the pion candidates. The average momenta of tracks used for this study is 1.8 GeV (2.8 GeV) for the electrons in the barrel (end-cap) region, and 1.6 GeV (2.2 GeV) for the pions in the barrel (end-cap).

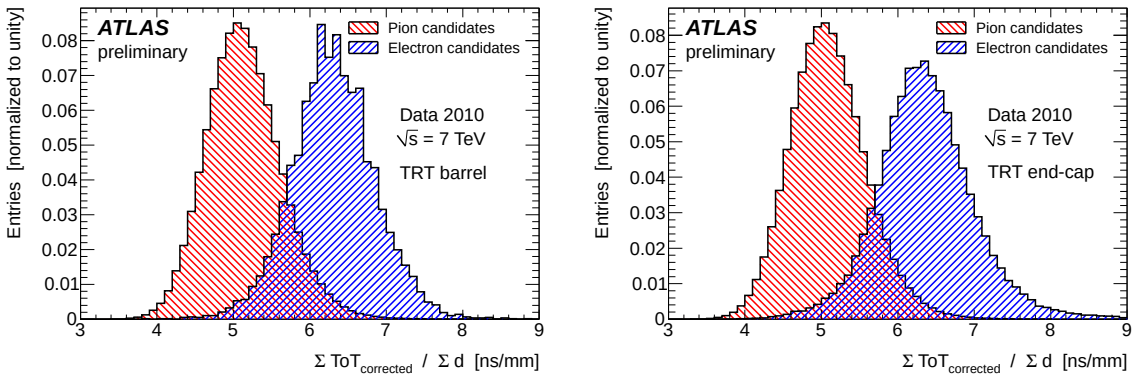

Figure 10: The average corrected time over threshold ($\mathrm{ToT}_{\mathrm{corrected}}$), divided by the average transverse track path length inside the straw. Only the distance along the straw dependence is taken into account with the current ToT corrections.

5.2 Identification of highly ionizing particles

The measurements sensitive to $\mathrm{d}E/\mathrm{d}x$ that are used to identify electrons can also be used to identify any highly ionizing particles. The ToT measurement in the TRT was used for one of the background estimation cross-checks in the ATLAS heavy ionizing stable massive particle (SMP) search with 2010 data [3]. The expected ionization loss from SMP is higher than for electrons, motivating a different choice of hits used to identify them. For studies of SMPs, all hits are required to have no "gaps" in the bit pattern, and a length of at least two time-bins. The tracks are required to have at least one pixel, at least six SCT, and at least 15 TRT hits. The range of $0 < |\eta| < 2$ includes both barrel and end-cap regions of the detector. Track impact parameters with respect to the primary vertex are required to satisfy $|d_0| < 1\,\mathrm{mm}$ and $|z_0 \sin(\theta)| < 1\,\mathrm{mm}$. A data set of approximately 17 million tracks collected with a minimum bias trigger during one run in May 2010 is used for this study.

The measured ToT is corrected for the dependence on the measured drift radius r and the η of the track. This correction is done separately for MC samples and data, using all tracks with $2\,\mathrm{GeV} < p < 10\,\mathrm{GeV}$. It is done in two independent steps: one for the r dependence and one for the η dependence. To correct for the r dependence, the mean ToT is obtained in bins of r, and subtracted from the measured value. Once the r dependence is corrected for, the mean ToT is studied as a function of the reconstructed track η, separately for the barrel and the end-caps. The two η dependencies are each fitted with a 5th order polynomial, and the results are used for η dependent corrections. Finally, the ToT-based estimator is shifted such that the corresponding distribution for hadrons is centered at "one" (3.12 ns bin). To obtain a ToT measurement for a track, the ToT measurements are averaged over all hits on track.

Figure 11 shows the ToT distributions after all corrections. The widths of the corrected distributions in data and MC simulation are similar. Figure 12 shows the same distribution as a function of track momenta. The bands at higher ToT correspond to protons and kaons that have higher $\mathrm{d}E/\mathrm{d}x$.

The relation between the corrected track ToT measurement and the track $\beta\gamma$ was determined from MC studies, as shown in Fig. 13 (a). The measured $\beta\gamma$ and momentum are used to measure the particle mass, $m = p/(\beta\gamma)$. The result for tracks with track-averaged, corrected ToT between $2 \times 3.12\,\mathrm{ns}$ and $5 \times 3.12\,\mathrm{ns}$ is shown in Fig. 13 (b). The average momenta of selected tracks is $p = 0.8\,\mathrm{GeV}$. The proton mass resolution for proton candidates included in this figure is found to be about 90 MeV.

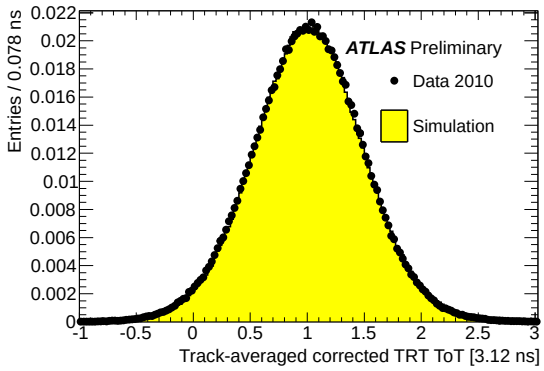

Figure 11: The distribution of track-averaged corrected ToT, in units of read-out time bins.

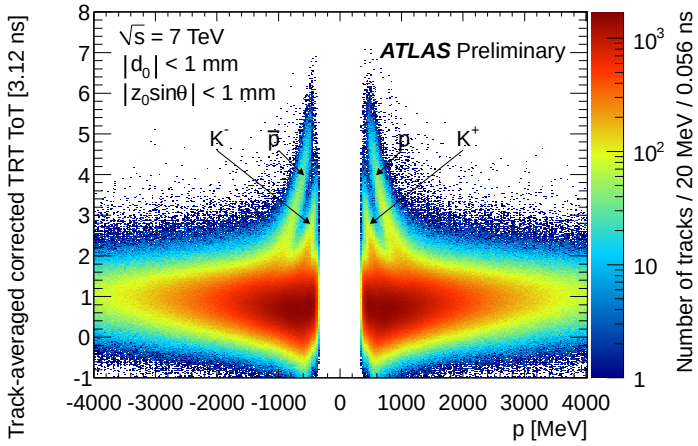

Figure 12: The track-averaged corrected ToT distribution, as a function of the track momenta.

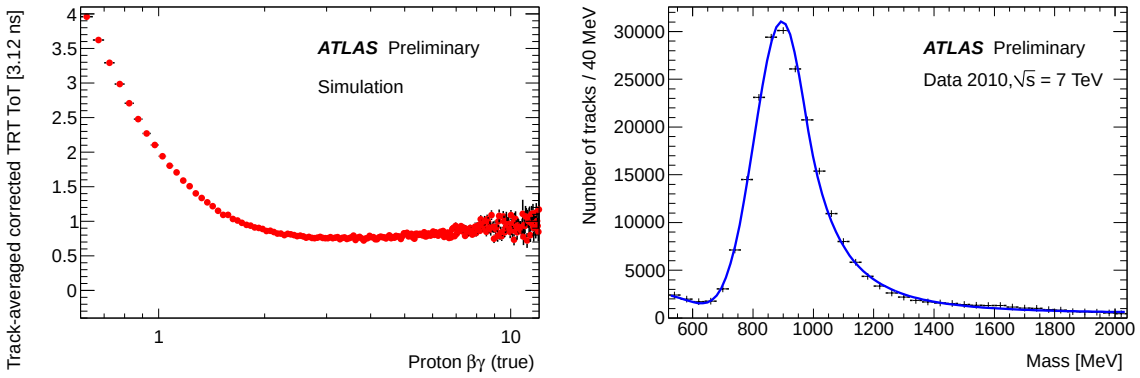

(a) (b)

Figure 13: The relation between the corrected track ToT measurement and the track $\beta\gamma$ is first obtained based on MC studies (a), and then applied to data to measure the mass of particles (b). The distribution of the reconstructed particle mass shown in Fig. (b) is fitted with a Crystal Ball function.

6 Combining HT and ToT measurements

The HT fraction and the ToT measurements can be combined to achieve the best electron identification performance. To combine the HT and ToT measurements, two likelihood functions are first formed based on the discriminating variables: one for HT, and one for ToT. Since the HT hits are not used for ToT discriminator, the two likelihoods are assumed to be independent, and are multiplied to form a single combined likelihood. The electrons are then selected by applying a cut on the combined likelihood.

To compare the performance in collision data with the expected performance reported in the ATLAS Technical Design Report [16], the performance of a selection criterion that gives 90% electron efficiency is used as a reference. A criterion that gives a 90% electron efficiency was determined in different momentum bins, and applied to the pion sample to determine the efficiency for pions to pass the same criterion. Figure 14 shows the pion misidentification probability $p_{\pi\to e}$ at 90% electron efficiency as a function of momentum. A larger 2010 data set was used for this figure in order to have better statistics for higher momentum electron candidates. The uncertainties were estimated by varying the selection criteria such that the electron efficiency changed by ±2%. It should be noted that any contamination of the pion sample with electrons above the TR threshold will systematically bias the estimate of $p_{\pi\to e}$ by roughly the same amount. The ToT-based selection improves the pion rejection at $p < 10$ GeV.

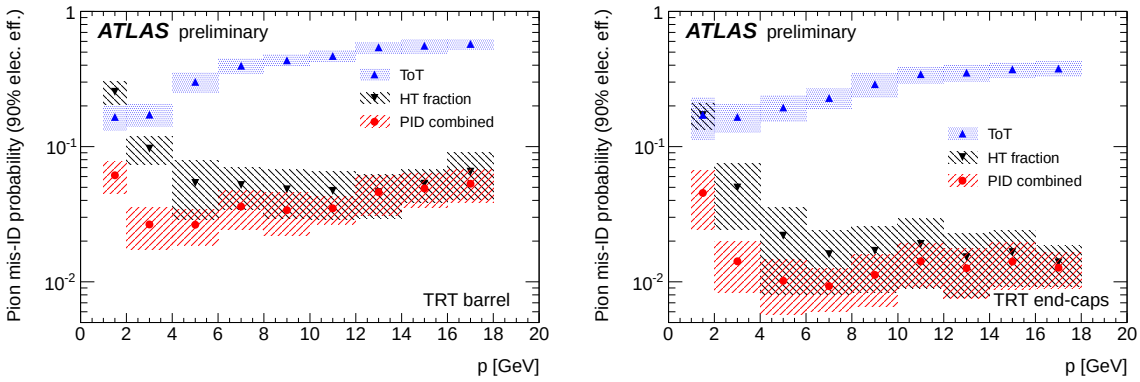

(a) $|\eta| < 0.625$ (b) $|\eta| > 1.057$

Figure 14: The pion misidentification probability for a selection criteria that gives 90% electron efficiency, as a function of momentum for the barrel (a) and end-cap (b) region of the detector.

7 Summary

Studies in the early collision data collected with the ATLAS detector have confirmed that electron identification based on transition radiation measured by the TRT is performing well, and in some detector regions even exceeds the performance obtained from the current detector simulation. The pion misidentification probability for selection criteria that give 90% electron efficiency is about 5% (rejection factor 20) for the majority of the detector and as low as $1-2$% in the best performing detector regions. Analysis of data from a dedicated run with different hardware threshold settings confirmed that the settings were close to their optimal value, and only a small change was applied in order to ensure stable performance under a wide range of operating conditions. The transition radiation measurement was used to identify electrons for the first W boson production cross section measurement by ATLAS [17], as well as for the W^+W^- cross section measurement [18] and other analyses such as a search for supersymmetry [19].

The time over threshold measurements can be used to further improve the electron-pion separation, in particular for tracks with momentum less than 10 GeV. It has been shown that this technique can also be successfully applied in searches for highly ionizing particles.

References

[1] ATLAS Collaboration, *The ATLAS Experiment at the CERN Large Hadron Collider*, JINST **3**, S08003 (2008).

[2] ATLAS collaboration, *Electron performance measurements with the ATLAS detector using the 2010 LHC proton-proton collision data*, ATLAS note CERN-PH-EP-2011-117.

[3] ATLAS Collaboration, *Search for stable hadronising squarks and gluinos with the ATLAS experiment at the LHC*, Phys. Lett. B **701**, 1-19 (2011).

[4] E. Abat et al., *The ATLAS Transition Radiation Tracker (TRT) proportional drift tube: design and performance*, JINST **3**, P02013 (2008).

[5] E. Abat et al., *ATLAS TRT Barrel Detector*, JINST **3**, P02014 (2008).

[6] E. Abat et al., *The ATLAS TRT end-cap detectors*, JINST **3**, P10003 (2008).

[7] E. Abat et al., *The ATLAS TRT electronics*, JINST **3**, P06007 (2008).

[8] ATLAS collaboration, *Calibration of the ATLAS Transition Radiation Tracker*, ATLAS note ATLAS-CONF-2011-006.

[9] ATLAS Collaboration, *The ATLAS Simulation Infrastructure*, Eur. Phys. J. **C70**, 823-874 (2010).

[10] S. Agostinelli et al. (GEANT4 Collaboration), *GEANT4: A simulation toolkit*, Nucl. Instrum. Meth. **A506**, 250-303 (2003).

[11] ATLAS collaboration, *Photon Conversions at* $\sqrt{s} = 900$ GeV *measured with the ATLAS Detector*, ATLAS note ATLAS-CONF-2010-007.

[12] ATLAS Collaboration, *dE/dx measurement in the ATLAS Pixel Detector*, ATLAS note ATLAS-CONF-2011-016.

[13] E. Klinkby, *W mass measurement and simulation of the Transition Radiation Tracker at the ATLAS experiment*, ATLAS PhD thesis CERN-THESIS-2008-071 (2008).

[14] ATLAS Collaboration, *The ATLAS Inner Detector commissioning and calibration*, Eur. Phys. J. C **70**, 787-821 (2010).

[15] ATLAS Collaboration, *Performance of the ATLAS Detector using First Collision Data*, JHEP **9**, 1-66 (2010).

[16] ATLAS Collaboration, *ATLAS detector and physics performance: Technical Design Report, Volume 1*, ATLAS note CERN-LHCC-99-014.

[17] ATLAS Collaboration, *Measurement of the* $W \to l\nu$ *and* $Z/\gamma^* \to ll$ *production cross sections in proton-proton collisions at* $\sqrt{s} = 7$ *TeV with the ATLAS detector*, JHEP **12**, 060 (2010).

[18] ATLAS Collaboration, *Measurement of the* W^+W^- *cross section in* $\sqrt{s} = 7$ *TeV pp collisions with ATLAS*, Phys. Rev. Lett. **107**, 041802 (2011).

[19] ATLAS Collaboration, *Search for supersymmetry using final states with one lepton, jets, and missing transverse momentum with the ATLAS detector in* $\sqrt{s} = 7$ *TeV pp collisions*, Phys. Rev. Lett. **106**, 131802 (2011).